Structure and dynamics of ND_3BF_3 in the solid and gas phases : a combined NMR, neutron diffraction, and Ab initio study

Penner, Glenn H.; Ruscitti, Bruno; Reynolds, Julie; Swainson, Ian

Publisher's version / Version de l'éditeur:
https://doi.org/10.1021/ic0203771
Inorganic Chemistry, 41, 26, pp. 7064-7071, 2002-11-26

Inorg. Chem. **2002**, *41*, 7064–7071

Structure and Dynamics of ND_3BF_3 in the Solid and Gas Phases: A Combined NMR, Neutron Diffraction, and Ab Initio Study

Glenn H. Penner,*,† Bruno Ruscitti,† Julie Reynolds,† and Ian Swainson‡

Department of Chemistry, University of Guelph, Guelph, Canada N1G 2W1, and NRC Canada, Steacie Institute for Molecular Sciences, Neutron Program for Materials Research, Chalk River, Canada K0J 1J0

Received June 3, 2002

The decrease in D→A bond lengths, previously reported for some Lewis acid/base complexes, in going from the gas to the solid phases is investigated by obtaining an accurate crystal structure of solid ND_3BF_3 by powder neutron diffraction. The B–N internuclear distance is 1.554(3) Å, 0.118 Å shorter than the most recent gas-phase microwave value and 0.121 Å shorter than the single molecule geometry optimized (1.672 Å, CISD/6-311++G-(d,p)) bond length. The crystal structure also shows N–D···F–B hydrogen bonds. The effects of this change in structure and of intermolecular hydrogen-bonding on nuclear magnetic shielding (i.e., chemical shifts) and the nuclear quadrupolar coupling constants (QCC) are investigated by ab initio molecular orbital and density functional theory calculations. These calculations show that the nitrogen (^{15}N and ^{14}N) and boron (^{11}B and ^{10}B) chemical shifts should be rather insensitive to changes in r_{BN} and that the concomitant changes in molecular structure. Calculations on hydrogen-bonded clusters, based on the crystal structure, indicate that H-bonding should also have very little effect on the chemical shifts. On the other hand, the ^{11}B and ^{14}N QCCs show large changes because of both effects. An analysis of the $^{10}B\{^{19}F\}$ line shape in solid $ND_3{}^{10}BF_3$ yields a ^{11}B QCC of ±0.130 MHz. This is reasonably close an earlier value of ±0.080 MHz and the value of ±0.050 MHz calculated for a $[NH_3BF_3]_4$ cluster. The gas-phase value is 1.20 MHz. Temperature-dependent deuterium T_1 measurements yield an activation energy for rotation of the ND_3 group in solid ND_3BF_3 of 9.5 ± 0.1 kJ/mol. Simulations of the temperature-dependent T_1 anisotropy gave an E_a of 9.5 ± 0.2 kJ/mol and a preexponential factor, A, of $3.0 \pm 0.1 \times 10^{12}$ s^{-1}. Our calculated value for a $[NH_3BF_3]_4$ cluster is 16.4 kJ/mol. Both are much higher than the previous value of 3.9 kJ/mol, from solid-state proton T_1 measurements.

Introduction

The charge transfer, Lewis acid−base complex, NH_3BF_3, was first prepared in the early 19th century[1] and has since been synthesized by countless students in introductory inorganic laboratories.[2] An early (1951) X-ray crystal structure provides what could best be described as estimates of r_{BN} (1.60 Å), r_{BF} (1.38 Å), and θ_{NBF} (107°).[3] A more recent, and higher quality, structure of the methylene chloride solvated 18-crown-6 ether complex of NH_3BF_3 has been reported.[4] To date no high quality structure, including accurate hydrogen positions, is available for solid NH_3BF_3. Determination of the gas-phase structure of NH_3BF_3 by rotational spectroscopy eluded researchers until the past decade.[5] This was due to the tendency of the vapor of the solid adduct to form $NH_2{=}BF_2$. It is evident from the X-ray and microwave structures that the BN bond length in NH_3-BF_3 is shorter in the solid state. This puts NH_3BF_3 in a class of donor−acceptor complexes in which the D→A bond length decreases significantly in going from the gas to the solid phases. Other examples where this bond length decrease is observed are as follows: NH_3BH_3,[6] $N(CH_3)_3BF_3$,[7] NH_3-SO_3,[8] $N(CH_3)_3SO_3$,[9] $N(CH_3)_3SO_2$,[10] CH_3CNBF_3,[11] and HC-NBF_3.[12] In the last case the decrease is particularly large at 0.835 Å!

* Author to whom correspondence should be addressed. E-mail: gpenner@uoguelph.ca.
† University of Guelph.
‡ Steacie Institute for Molecular Sciences.

(1) (a) Gay-Lussac, J. L.; Thénard, J. L. *Mem. Phys. Chim. Soc. d'Arcueil* **1809**, *2*, 210. (b) Davy, J. *Philos. Trans.* **1812**, *102*, 365.
(2) Marr, G.; Rockett, B. W. *Practical Inorganic Chemistry*; Van Nostrand Reinhold: London, 1972.
(3) Hoard, J. L.; Geller, S.; Cashin, W. M. *Acta Crystallogr.* **1951**, *4*, 396.
(4) Colquhoun, H. M.; Jones, G.; Maud, J. M.; Stoddart, J. F.; Williams, D. J. *J. Chem. Soc., Chem. Commun.* **1984**, 63.
(5) Legon, A. C.; Warner, H. E. *J. Chem. Soc., Chem. Commun.* **1991**, 1397.

10.1021/ic0203771 CCC: $22.00
Published on Web 11/26/2002

There have been three recent ab initio calculations on NH_3BF_3. Fujiang et al. report an MP2/TZ2P geometry optimization of NH_3BF_3 and calculate the BN bond length dependence of the energy, dipole moment, and electric field gradients at N and B.[13] Jonas and Frenking give r_{BN} for optimized geometries at various levels, including MP3/6-31(d,p) and QCISD/6-31G(d,p).[14] Jonas et al. have produced a comprehensive theoretical study of several Lewis acid−base complexes including NH_3BF_3. Aside from a geometry optimization of NH_3BF_3 at several levels of theory, they showed that r_{BN} decreases by about 0.05 Å upon dimerization.[15]

The dynamics of the NH_3 and BF_3 groups in solid NH_3BF_3 have been investigated by variable temperature ^1H and ^{19}F spin−lattice time (T_1) measurements.[16] This study yields activation energies for rotation of the BF_3 and NH_3 groups of 25.02 and 3.91 kJ/mol. This latter value seems unusually small considering the possibility of N−H···F−B hydrogen-bonding. Turning to the gas phase, an A,E splitting in the rotational spectrum of about 60 kHz led Legon and Warner to estimate an internal rotational barrier, V_3, of approximately 7 kJ/mol.[5] This is nearly twice the E_a found in the solid.

NMR parameters are known to be sensitive probes of molecular structure and dynamics. The isotropic ^{11}B and ^{19}F chemical shifts of NH_3BF_3 have been measured in solution.[17] In addition, the ^{11}B nuclear quadrupolar coupling constant has been reported for solid NH_3BF_3.[18] The spectrum was recorded at low field (1.41 T) in CW mode without ^{19}F decoupling. The rather poor quality spectrum gave an ^{11}B QCC of 80 ± 8 kHz. This value is over an order of magnitude smaller than that measured in the gas phase (about 1.2 MHz, depending on the torsional state).[5]

The purpose of this study is to determine the molecular structure of solid NH_3BF_3 including accurate hydrogen positions, to determine the activation parameters for ammonia group rotation in solid ND_3BF_3 by deuterium T_1 and T_1 anisotropy measurements, and to redetermine the boron quadrupolar coupling constant in solid NH_3BF_3. We will also employ ab initio molecular orbital and density functional theory (DFT) methods to calculate the barrier to rotation of the NH_3 group, the N and B nuclear quadrupolar coupling constants, and the chemical shielding (i.e., shift) parameters. These will be compared to experimental values available in the gas and solid phases.

Theoretical Background

Deuterium Line Shapes. The solid-state deuterium NMR spectral line shape is dominated by the quadrupolar interaction. This is the interaction between the nuclear quadrupole moment, eQ, and the largest component of the electric field gradient (efg) tensor at the nucleus, eq_{zz}. The quadrupolar coupling constant, χ, which is a measure of the strength of the quadrupolar interaction, is given as

$$\chi = \frac{e^2 q_{zz} Q}{h} \tag{1}$$

The line shape is also influenced by the asymmetry parameter of the efg tensor, η, which is defined as the difference between the two smaller principal components of the diagonalized efg tensor, eq_{xx} and eq_{yy}, with respect to the largest component, eq_{zz}

$$\eta = \frac{eq_{xx} - eq_{yy}}{eq_{zz}} \tag{2}$$

For the molecule studied here, the η values are very small (<0.1), and it will be assumed that the efg is axially symmetric along the N−D bond. In that case, the spectrum from a deuterium nucleus located in a static N−D bond consists of a doublet with spacing

$$\Delta\nu = \frac{3e^2 q_{zz} Q}{4h}(3\cos^2\alpha - 1) \tag{3}$$

where α is the angle between the X−D bond and the static magnetic field, B_0. In powdered samples, the line shape is determined by the random distribution of the X−D bond orientations with respect to B_0, yielding a typical Pake doublet with a characteristic splitting between peaks ($\alpha = 90°$) of $3\chi/4$ and shoulders ($\alpha = 0°$) separated by $3\chi/2$ (see Figure 4). The effects of motion on the deuterium powder spectrum are 2-fold. First the width of the spectral line is narrowed by the motion. In the case of a jumping motion of the X−D bond between three or more equally populated sites, as is expected for ND_3 and BD_3 groups, η is averaged to zero and, if the motion is fast as compared to the quadrupolar interaction (i.e., $>10^6$ s^{-1}), the quadrupolar splitting, $\Delta\nu$, is reduced to

$$\Delta\nu_{eff} = \frac{3\chi^2}{8}(3\cos^2\theta - 1) \tag{4}$$

where θ is the angle between the X−D bond and the rotational axis. If the motional rate, k, is of the order of P ($\sim 10^4 - 10^6$ s^{-1}) the spectral line shape is severely distorted because of the large T_2 anisotropy associated with the

(6) Klooster, W. T.; Koetzle, T. F.; Siegbahn, P. E. M.; Richardson, T. B.; Crabtree, R. H. **1999**, *121*, 6337.
(7) (a) Geller, S.; Hoard, J. L. *Acta Crystallogr.* **1951**, *4*, 399. (b) Iijime, K.; Shibata, S. *Bull. Chem. Soc. Jpn.* **1979**, *52*, 711. (c) Cassoux, P.; Kuczowski, R. L.; Serafini, A. *Inorg. Chem.* **1977**, *16*, 3005.
(8) (a) Bats, J. W.; Coppens, P.; Koetzle, T. F. *Acta Crystallogr.* **1977**, *B33*, 37. (b) Canagaratna, M.; Phillips, J. A.; Goodfriend, H.; Leopold, K. R. *J. Am. Chem. Soc.* **1996**, *118*, 5290.
(9) (a) Morris, A. J.; Kennard, C. H. L.; Hall, J. R.; Smith, G.; White, A. H. *Acta Crystallogr.* **1983**, *C39*, 81. (b) Fiacco, D. L.; Leopold, K. R. *Inorg. Chem.* **2000**, *39*, 37.
(10) (a) Van Der Helm, D.; Childs, J. D.; Christian, S. D. *J. Chem. Soc., Chem. Commun.* **1969**, 887. (b) Oh, J. J.; LaBarge, M. S.; Matos, J.; Kamp, J. W.; Hillig, K. W.; Kuczkowski, R. L. *J. Am. Chem. Soc.* **1991**, *113*, 4732.
(11) Swanson, B.; Shriver, D. F.; Ibers, J. A. *Inorg. Chem.* **1969**, *8*, 2182.
(12) (a) Cabaleiro-Lago, E. M.; Rios, M. A. *Chem. Phys. Lett.* **1998**, *294*, 272. (b) Burns, W. A.; Leopold, K. R. *J. Am. Chem. Soc.* **1993**, *115*, 11622.
(13) Fujiang, D.; Fowler, P. W.; Legon, A. C. *J. Chem. Soc., Chem. Commun.* **1995**, 113.
(14) Jonas, V.; Frenking, G. *J. Chem. Soc., Chem. Commun.* **1994**, 1489.
(15) Jonas, V.; Frenking, G.; Reetz, M. T. *J. Am. Chem. Soc.* **1994**, *116*, 8741.
(16) Yamauchi, J.; McDowell, C. A. *J. Chem. Phys.* **1981**, *75*, 577.
(17) (a) Heitsch, C. W. *Inorg. Chem.* **1965**, *4*, 1019. (b) Dugan, C. H.; Van Wazer, J. R. *Compilation of ^{19}F NMR Chemical Shifts*; Wiley-Interscience: Toronto, 1970.
(18) Olliges, J.; Lötz, A.; Voitländer. *J. Magn. Reson.* **1986**, *69*, 302.

dynamic process. The distorted line shapes can readily be simulated for a given combination of χ, θ, and k.

Deuterium Relaxation Times. The spin−lattice relaxation time, T_1, characterizes the return of the bulk magnetization to its equilibrium state after a perturbing pulse. Relaxation is stimulated by time-dependent nuclear spin interactions and is most efficient when these fluctuations occur at the resonance frequency of the nucleus. For deuterons, the primary source of these fluctuating fields is the time-dependent part of the quadrupolar interaction.

When the reorientational motion can be described by an exponential correlation function and the temperature dependence of the correlation time follows Arrhenius behavior, the rate of relaxation may be fit to the following equations:

$$\frac{1}{T_1} = K\left(\frac{\tau_c}{1+\omega_0^2\tau_c^2} + \frac{4\tau_c}{1+4\omega_0^2\tau_c^2}\right) \quad (5)$$

$$\tau_c = \tau_\infty \exp\left(\frac{E_a}{RT}\right) \quad (6)$$

where τ_c is the correlation time for the motion ($\tau_c \propto k^{-1}$), τ_∞ is its value at infinite temperature, and ω_0 is the Larmor precession frequency. In addition, E_a is the activation energy for the motion influencing T_1, and K depends on the strength of the dominant nuclear spin interaction (in this case χ^2) and the exact nature of the reorientational motion. For jumps of the X−D bond between three or more equivalent positions oriented at an angle θ about the rotational axis, K is given by

$$K = \frac{9\pi^2\chi^2}{20}(3\cos^2\theta - 1) \quad (7)$$

In this case, if a plot of $\ln(T_1)$ versus inverse temperature is made, one often sees a V-shaped curve, with a T_1 minimum at $\tau_0\omega_c = 0.62$. There is, in general, much information to be extracted from this T_1 plot. The slope of the curve on either side of the T_1 minimum is characteristic of the activation energy for the motion influencing T_1. The intercept at $1/T = 0$ yields a value for τ_∞, while the depth of the minimum can be used to determine a value for the effective quadrupolar coupling constant. Note that knowledge of τ_∞ and E_a allows calculation of the motional rate at any temperature through eq 6.

Boron-10 Line Shapes. For the case where $\eta = 0$ the ^{10}B line shape consists of three pairs of Pake doublets, for the $0 \leftrightarrow \pm 1$, $\pm 1 \leftrightarrow \pm 2$, and $\pm 2 \leftrightarrow \pm 3$ transitions (compare to the deuterium case that has only one, $0 \leftrightarrow \pm 1$, set of transitions, hence one doublet). A simulation of such a set of doublets is shown in Figure 11. The separation between the peaks or horns of the Pake doublets is $\chi/20$, $3\chi/20$, and $5\chi/20$, respectively.

Experimental Section

Three different isotopomers were prepared for this study. Initially a sample of $N^2H_3BF_3$ (hereafter referred to as ND_3BF_3) was used for the deuterium line shape and T_1 work. Later a sample of $N^2H_3{}^{11}BF_3$ was required for the neutron diffraction structure determination. To maximize the signal-to-noise ratio in the ^{10}B study, a sample of $ND_3{}^{10}BF_3$ was prepared. Deuterium was included in this sample to reduce the ^{10}B−^{1}H dipolar line broadening in the ^{10}B spectrum. This allows us to perform a double resonance $^{10}B\{^{19}F\}$ experiment rather than the more demanding $^{10}B\{^1H,^{19}F\}$ experiment.

All three isotopomers were prepared by bubbling ammonia-d_3 gas (MSD isotopes) through a solution of $^{11}BF_3$ or $^{10}BF_3$ in ether (Aldrich). The solid product simply precipitated out of solution, was filtered, and was washed with dry ether. The sample is stable in air, but the deuterium will eventually be replaced by hydrogen when exposed to moisture. The purity of the samples was checked by ^{19}F and ^{11}B (or ^{10}B) spectra of the solid dissolved in D_2O. Some samples contained an impurity that was determined to be NH_4BF_4.

Structural data for $ND_3{}^{11}BF_3$ were determined by powder neutron diffraction measurements at 5 K. The powder samples were contained in vanadium tubes of 5 mm i.d. and wall thickness of 0.18 mm, which were filled with helium gas. The samples were rotated about one axis throughout data collection to improve averaging over crystallite orientations. The experiments were done on the C2 Dualspec high-resolution powder diffractometer at the NRU reactor at Chalk River, and data were collected from 5 to 120° with a step size of 0.025°. The monochromator was Si(531), and the takeoff angle was $2\theta = 92.7°$. The neutron wavelength of 1.3284 Å was calibrated using a separate Si powder standard. The sample temperature was controlled by a commercially available open cycle design helium cryostat, with separate silicon diodes for the measurement and control of temperature. Structure refinement was carried out using the GSAS Rietveld refinement code.[19]

Deuterium spectra, obtained at 30.74 MHz on a Bruker ASX-200, of a 100 mg sample of solid ND_3BF_3 employed a quadrupolar echo pulse sequence.[20] The spectra were obtained at temperature intervals of about 20 K from room temperature (291 K) down to 110 K. Deuterium spin−lattice relaxation times were measured at temperatures down to 110 K using an inversion−recovery quadrupolar echo pulse sequence. For each temperature 16 different variable delays were used. The T_1 at each temperature was determined using the TONE program. For all deuterium experiments a $\pi/2$ pulse of 2.6 μs, a pulse spacing of 40 μs, and a relaxation delay of at least $5T_1$ were used. After each temperature change a period of 15 min was allowed for the sample to reach thermal equilibrium. A Eurotherm B-VT2000 was used for temperature regulation, and the sample temperature was checked before each run by lowering a thermocouple down the bore of the magnet into the sample compartment.

Solid-state ^{10}B spectra were obtained on a Chemagnetics CMX Infinity ($B_0 = 4.7$ T, $\nu_0(^{10}B) = 21.5$ MHz) NMR spectrometer. Single pulse experiments were used with pulses of 2 μs (90° pulse was 5.5 μs). The spectra were acquired with ^{19}F high power decoupling.

Theoretical calculations were performed with Gaussian 98.[21] Nuclear quadrupolar coupling constants were obtained from the calculated electric field gradients via the relationship $\chi = -235Qq_{zz}$, where χ is the QCC in kiloHertz, Q is the nuclear quadrupole moment in millibarns, and q_{zz} is the largest calculated electric field gradient at the nucleus of interest in atomic units. The Q values recently published by Pyykko were used.[22] The values used in this study are as follows: $Q(^2H) = 2.86$, $Q(^{11}B) = 40.59$, $Q(^{10}B) = 84.59$, and $Q(^{14}N) = 20.1$.

(19) Larson, A. C.; Von Dreele, R. B. *Report No. LA-UR-86-748*; Los Alamos National Laboratory: Los Alamos, 1987.
(20) Davis, J. H.; Jeffrey, K. R.; Bloom, M.; Valic, M. I.; Higgs, T. P. *Chem. Phys. Lett.* **1976**, *42*, 390.

The deuterium line shapes and T_1 anisotropies were simulated with the program MXET1.[23] The ^{10}B spectrum was simulated with the WSOLIDS software.[24]

Results and Discussion

Neutron Diffraction Structure of ND_3BF_3. The analysis of the neutron diffraction pattern was accomplished by starting with the published X-ray structure and refining the structural parameters, including the deuterium positions. The results of the refinement of the structure of solid ND_3BF_3 are summarized in Tables 1−6. Figure 1 shows the observed and calculated powder patterns. The unit cell, which contains eight molecules, is depicted in Figure 2. The crystal structure indicates that each fluorine atom on one molecule is hydrogen-bonded to one deuterium atom from each of three neighboring molecules, thus forming an infinite network of hydrogen bonds throughout the crystal lattice. This arrangement is shown in Figure 3a. Similarly, each deuteron of a ND_3BF_3 molecule is hydrogen-bonded to one fluorine from each neighboring molecule. This arrangement is shown in Figure 3B. Table 7 compares our neutron diffraction analysis to the earlier results of Geller et al.[3] The most important difference is that the neutron diffraction analysis yields a B−N bond that is shorter by 0.046 Å.

Deuterium NMR Spectra and T_1. The ^2H line shape of solid ND_3BF_3 does not change in the temperature region between 300 and 110 K. This spectral line shape (see Figure 4 for an example) is consistent with a ND_3 group rapidly rotating at a rate, k, greater than 10^8 s^{-1}. If one assumes a rapid interchange between the three N−D deuterons and uses the neutron diffraction structure, eq 4 yields a $\chi(^2H)$ of 184 kHz for the nonexchanging deuterons. Values for other ND_3 donor−acceptor complexes are 198 ± 5 kHz for ND_3BH_3[25] and 162 ± 5 kHz for ND_3SO_3.[26] The deuterium QCC is a local property and is relatively independent of the acceptor group. On the other hand, it is rather sensitive to N−D···X−A interactions. For example, gas-phase rotational spectra and molecular orbital calculations show that $\chi(^2H)$ for isolated NH_3 is 290.6 kHz, whereas solid-state NMR experiments yield a $\chi(^2H)$ value of 156 kHz.[27] Similarly, our calculations of $\chi(^2H)$ for single molecules of NH_3BF_3 give values of 252 (B3LYP/6-311++G**) and 255 kHz (MP2/6-311++G**). Evidently there is a significant intermolecular N−H···F−B interaction, as implied by the neutron diffraction structure, which lowers the deuterium QCC. Details of the calculations of hydrogen-bonding effects on $\chi(^2H)$ in ND_3BF_3 will be presented later (vide infra).

Table 1

	atomic positions		
atom	*x*	*y*	*z*
B11	0.1608(7)	0.1062(6)	0.1686(6)
F12	0.0748(9)	−0.0477(8)	0.1740(7)
F13	0.3091(7)	0.0886(7)	0.0900(8)
F14	0.1895(9)	0.1662(8)	0.3089(8)
N15	0.0466(5)	0.2369(5)	0.0908(4)
D16	0.1016(11)	0.3537(9)	0.0932(9)
D17	−0.0665(11)	0.2477(9)	0.1387(6)
D18	0.0265(11)	0.2067(10)	−0.0123(7)

Table 2

Intramolecular Distances (Å)			
B11−F12	1.400(8)	N15−D16	1.024(7)
B11−F13	1.393(9)	N15−D17	1.007(9)
B11−F14	1.394(9)	N15−D18	0.991(7)
B11−N15	1.554(5)		

A plot of the deuterium T_1 as a function of sample temperature is shown in Figure 5. A low-temperature T_1 minimum could not be reached with our apparatus. This is consistent with the ND_3 rotational rate being in excess of 10^8 s^{-1} at temperatures above 110 K. The slope of the ln T_1 versus $1/T$ plot gave an activation energy of 9.1 ± 0.1 kJ/mol. Since the T_1 minimum could not be reached, it was not possible to determine the temperature-dependent rates for ND_3 rotation. In this case the alternative is to measure the T_1 anisotropy.[28] For a three-site exchange the anisotropy in the rate of relaxation of the powder line shape is dependent on the exchange rate. The inversion recovery deuterium spectra for one temperature are shown in Figure 6. As can be seen, the shoulders of the spectral line shape relax faster than the peaks. A plot of ln k versus $1/T$ is shown in Figure 7. A linear regression yields E_a = 9.5 ± 0.2 kJ/mol and a preexponential factor, A, of 3.0 ± 0.1 × 10^{12} s^{-1} for rotation of the ND_3 group. Earlier proton T_1 measurements provide E_a and A values of 3.91 kJ/mol and 8.99 × 10^{10} s^{-1}, respectively.[16] Although our results are not consistent with these numbers, there is agreement in E_a between our independent T_1 and T_1 anisotropy measurements. The preexponential factor, A, also known as the frequency factor or attempt frequency, is often identified with the torsional frequency for that motion. The attempt frequency for rotational motion of the ND_3 group, A, is in good agreement with the torsional frequency, ν_6, of 5.7 × 10^{12} s^{-1} obtained from the far-infrared spectrum of solid ND_3BF_3.[29]

Barrier to Internal Rotation. The gas-phase barrier to internal rotation in NH_3BF_3 has been estimated to be 7 kJ/mol.[5] Fluorine-19 and proton T_1 measurements yield barriers

(21) Frisch, M. J.; Trucks, G. W.; Schlegel, H. B.; Scuseria, G. E.; Robb, M. A.; Cheeseman, J. R.; Zakrzewski, V. G.; Montgomery, J. A., Jr.; Stratmann, R. E.; Burant, J. C.; Dapprich, S.; Millam, J. M.; Daniels, A. D.; Kudin, K. N.; Strain, M. C.; Farkas, O.; Tomasi, J.; Barone, V.; Cossi, M.; Cammi, R.; Mennucci, B.; Pomelli, C.; Adamo, C.; Clifford, S.; Ochterski, J.; Petersson, G. A.; Ayala, P. Y.; Cui, Q.; Morokuma, K.; Malick, D. K.; Rabuck, A. D.; Raghavachari, K.; Foresman, J. B.; Cioslowski, J.; Ortiz, J. V.; Stefanov, B. B.; Liu, G.; Liashenko, A.; Piskorz, P.; Komaromi, I.; Gomperts, R.; Martin, R. L.; Fox, D. J.; Keith, T.; Al-Laham, M. A.; Peng, C. Y.; Nanayakkara, A.; Gonzalez, C.; Challacombe, M.; Gill, P. M. W.; Johnson, B. G.; Chen, W.; Wong, M. W.; Andres, J. L.; Head-Gordon, M.; Replogle, E. S.; Pople, J. A. *Gaussian 98*, revision A.3; Gaussian, Inc.: Pittsburgh, PA, 1998.
(22) Pyykko, P. *Mol. Phys.* **2001**, *99*, 1617.
(23) Greenfield, M. S.; Ronemus, A. D.; Vold, R. L.; Vold, R. R.; Ellis, P. D.; Raidy, T. R. *J. Magn. Reson.* **1987**, *72*, 89.
(24) Eichele, K.; Wasylishen, R. E. *WSOLIDS NMR Simulation Package*, version 1.17.26, 2000.
(25) Laaksonen, A.; Wasylishen, R. E. *Z. Naturforsch.* **1995**, *50A*, 137.
(26) Penner, G. H.; Chang, Y. C. P.; Hutzal, J. *Inorg. Chem.* **1999**, *38*, 2868.
(27) Penner, G. H.; Chang, P.; Grandin, H. M. Unpublished results.
(28) (a) Torchia, D. A.; Szabo, A. *J. Magn. Reson.* **1982**, *49*, 107. (b) Wittebort, R. J.; Olejniczak, E. T.; Griffen, R. G. *J. Chem. Phys.* **1987**, *86*, 5411.
(29) Anderson, A.; Bobbie, B. A. *Spectrosc. Lett.* **1978**, *11*, 939.

Table 3

Intramolecular Angles (deg)					
F12−B11−F13	110.4(5)	F12−B11−F14	110.2(6)	F12−B11−N15	108.03(7)
F13−B11−F14	112.0(6)	F13−B11−N15	109.02(6)	F14−B11−N15	107.16(4)
B11−N15−D16	109.94(8)	B11−N15−D17	112.36(7)	B11−N15−D18	111.99(5)
D16−N15−D17	107.8(8)	D16−N15−D18	108.0(8)	D17−N15−D18	107.1(7)

Table 4

Intermolecular D····F Distances (Å)		
D16····F23	1.994(9)	$^1/_2 - x$, $^1/_2 + y$, z
D17····F84	2.107(11)	$-^1/_2 + x$, y, $^1/_2 - z$
D18····F32	2.110(10)	$-x$, $-y$, $-z$

Table 5

Intermolecular Angles (deg)[a]	
N15−D16····F23	175.11
N15−D17····F84	154.32
N15−D18····F32	151.70

[a] Obtained using PLUTON[33] and does not provide esd values.

Table 6

Lattice Parameters	
a, Å	7.9790(4)
b, Å	7.9250(4)
c, Å	9.1956(5)
α, deg	90.00
β, deg	90.00
γ, deg	90.00
vol, Å^3	581.48(5)
Agreement Factors	
R_{ex}	1.01%
R_{wp}	3.62%
R_p	2.64%
Thermal Parameters (10^{-2})[a]	
U_1, Å^2	0.012
U_2, Å^2	0.295
U_3, Å^2	0.479
U_4, Å^2	1.315

[a] These values were refined but damped during the analysis.

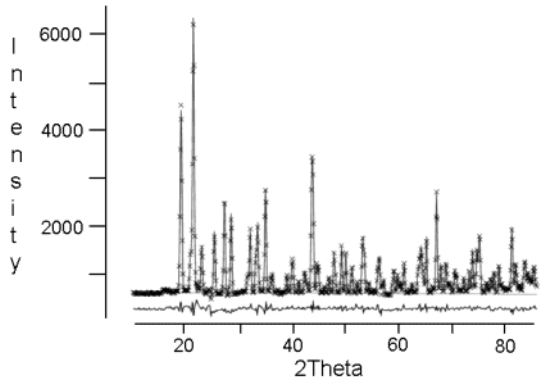

Figure 1. Neutron diffraction intensity profile and calculated fit for solid ND_3BF_3 at 5 K. The upper part of the diagram shows the observed and calculated profiles, and the lower part of the diagram shows the difference between observed and calculated profiles.

for rotation of the BF_3 and NH_3 groups in the solid as 25.0 and 3.91 kJ/mol, respectively, while our deuterium T_1 anisotropy measurements give a value of 9.5 kJ/mol for NH_3 rotation. The internal rotational barrier in isolated NH_3BF_3 is exclusively due to intramolecular interactions between the N−H and the B−F bonds. In the solid one must take into account the decrease in the B−N bond length and intermolecular N−H···F−B hydrogen-bonding. MP2 and B3LYP calculations, using the 6-311++G(d,p) basis set and the gas-phase bond length of 1.672 Å, yield E_a values of 4.5 and 3.5 kJ/mol, respectively. If the bond length is shortened to the solid-state value of 1.551 Å, these values increase to 7.0 and 5.6 kJ/mol. Figure 8 shows the calculated barrier height, V_3, as a function of r_{BN}. These curves can be fit to the equation $V_3 = Ae^{-Br}$. The MP2 calculations are best fit with A and B values of 2330 ± 70 kJ/mol and −3.75 ± 0.02, whereas the B3LYP values were 2080 ± 60 kJ/mol and −3.82 ± 0.02. The effect of hydrogen-bonding is much more difficult to calculate. As a first approximation one can start with the tetramer shown in Figure 3B and calculate the energy profile as the NH_3 group is rotated. Such a calculation assumes that the fluorine atoms of the three neighboring molecules are essentially stationary as the NH_3 group rotates. Our deuterium T_1 measurements yield a rate of 6.2×10^{10} s^{-1} for the three-site jumps of the NH_3 group in solid NH_3-BF_3 at 295 K. Earlier ^{19}F T_1 measurements provide a rate of 3.9×10^7 s^{-1} for the BF_3 rotational rate; a factor of about 1600 slower. An additional simplification is that the structure is not allowed to relax during the rotation of the NH_3 group. A B3LYP/6-311++G** calculation yields a barrier of 16.4 kJ/mol. The relative energy as a function of rotational angle is shown in Figure 9. The points nearly follow the equation $V(\theta) = 16.4 \sin^2(3\theta/2)$ (also shown in Figure 9). If the structure were allowed to relax during the NH_3 group rotation, the barrier would be expected to decrease by a few kiloJoules per mole, bringing the calculated V_3 closer to our experimental E_a value. One can also use the torsional vibrational frequency to estimate the barrier, V_3. If a high

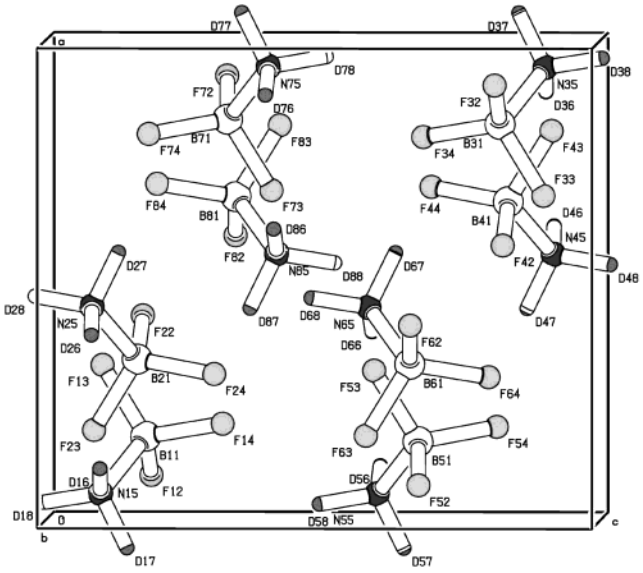

Figure 2. Crystallographic unit cell for solid ND_3BF_3.

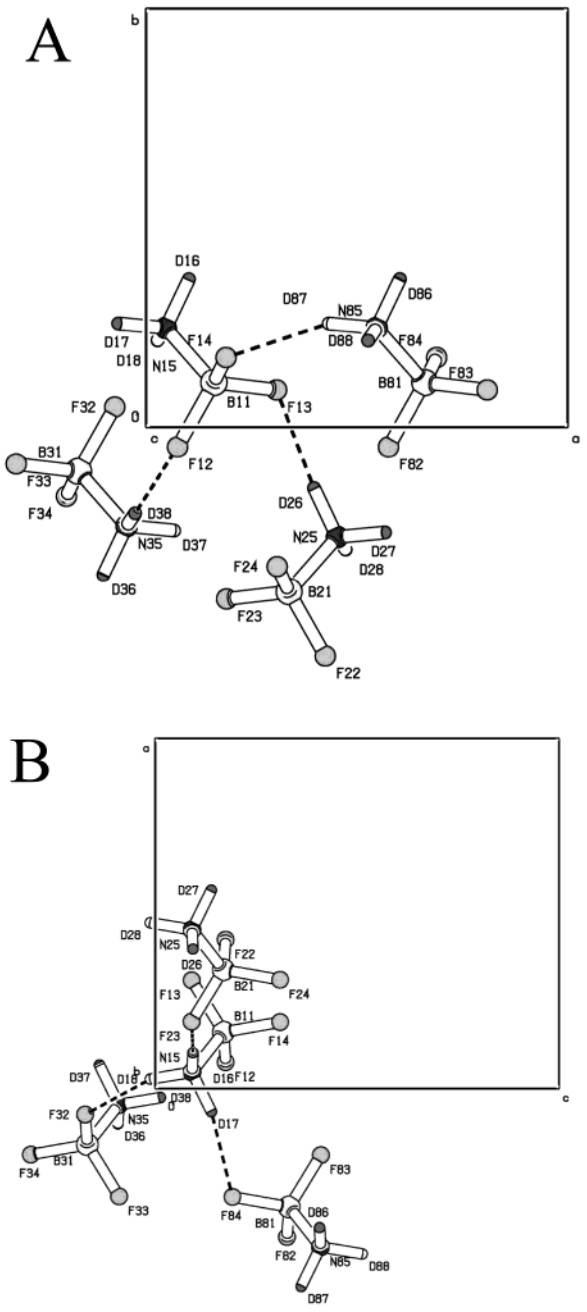

Figure 3. (A) Tetramer cluster showing one BF_3 group and the surrounding hydrogen-bonded molecules. (B) Tetramer cluster showing one ND_3 group and the surrounding hydrogen-bonded molecules.

Table 7

Lattice Parameters		
	our results	Geller et al.
space group	*Pbca*	*Pbca*
a, Å	7.9790(4)	8.22(3)
b, Å	7.9250(4)	8.11(3)
c, Å	9.1956(5)	9.31(3)
α, deg	90.00	90.00
β, deg	90.00	90.00
γ, deg	90.00	90.00
vol, Å^3	581.48(5)	620(7)
r_{NB}, Å	1.554(5)	1.60(5)

barrier is assumed, the potential function $V_3 \sin^2(3\theta/2)$ is replaced by $3V_3\theta^2/2$, and a harmonic oscillator Schrödinger

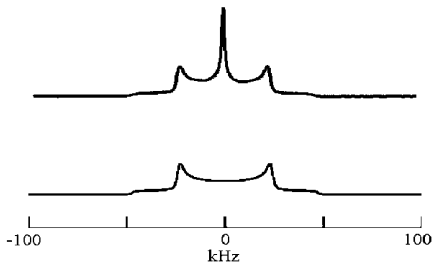

Figure 4. Experimental (upper) and simulated (lower) deuterium NMR spectrum of solid ND_3BF_3. The narrow peak in the center of the experimental spectrum is due to ND_4BF_4.

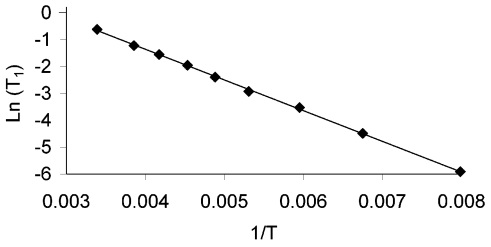

Figure 5. Plot of the deuterium ln T_1 vs inverse temperature for solid ND_3BF_3.

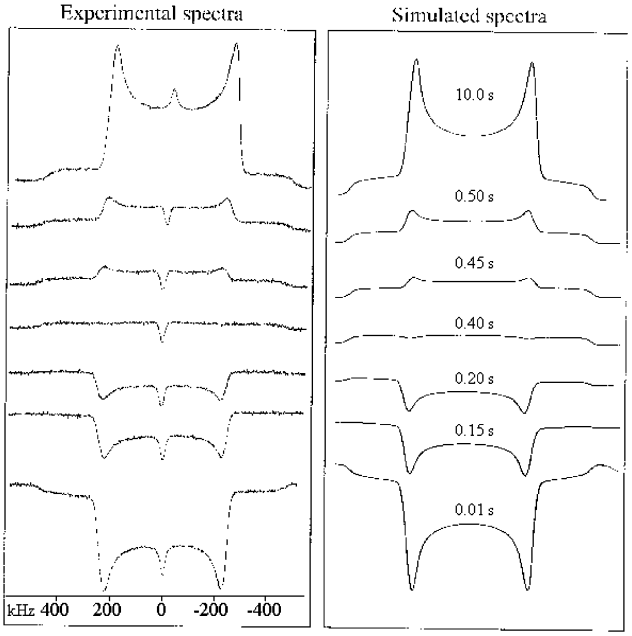

Figure 6. Deuterium inversion recovery spectra for solid ND_3BF_3 at 290 K and simulated spectra for different values of the interpulse spacing.

equation can be solved to give

$$V_3 = \frac{8}{9}\pi^2 I_r \nu^2$$

where I_r is the reduced moment of inertia for the rotation of the ND_3 group; $I_r = 3m_D r_{ND} \sin\theta$.[30] The previously measured torsional frequency in solid ND_3BF_3 gives a V_3 value of about 19 kJ/mol. Since the model used to obtain this number assumes a very high barrier to rotation, this number is an overestimation of V_3. Either way, our calculated and experimental values and the value estimated from the torsional

(30) Lister, D. G.; MacDonald, J. N.; Owen, N. L. *Internal Rotation and Inversion*; Academic Press: London, 1978.

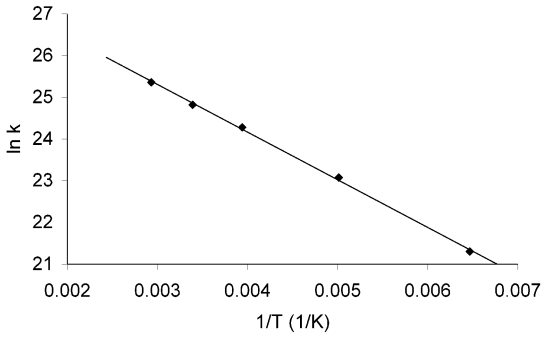

Figure 7. Plot of ln k vs $1/T$ for the rotation of the ND_3 group in solid ND_3BF_3.

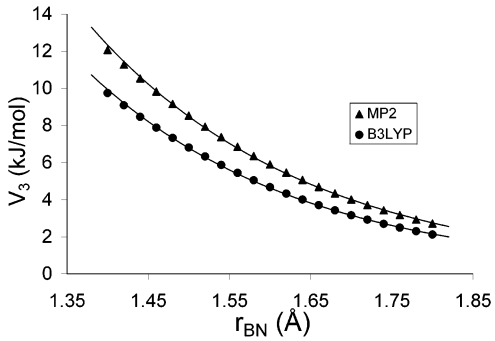

Figure 8. Plot of the calculated barrier height in gas-phase NH_3BF_3 as a function of B−N distance, r_{BN}. The solid curve is a fit to the equation $V_3 = Ae^{-Br}$.

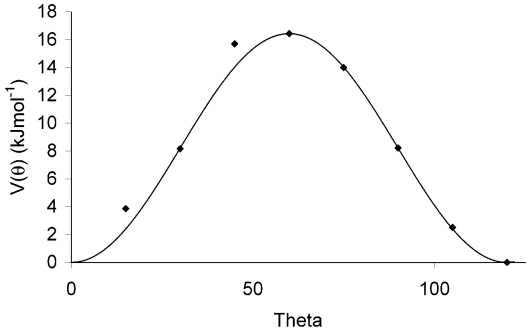

Figure 9. Plot of the calculated (B3LYP/6-311++G(d,p)) relative energies for the rotation of the NH_3 group in the tetramer depicted in Figure 3B. The solid curve is the equation $V(\theta) = 16.4 \sin^2(3\theta/2)$.

frequency for the barrier to NH_3 rotation in solid NH_3BF_3 are all significantly higher than the earlier solid-state experimental values.[16]

Boron, Nitrogen, and Deuterium Quadrupolar Coupling Constants. Calculations (B3LYP/6-311++G(d,p)) of ^{14}N and ^{11}B nuclear quadrupolar coupling constants were performed for boron−nitrogen bond lengths ranging from 1.4 to 1.8 Å, with optimization of all other structural parameters. The results are shown in Figure 10. The ^{14}N QCC appears to be rather insensitive to changes in r_{BN}, and no clear trend is discernible. On the other hand, the ^{11}B QCC changes significantly and, in fact, passes through zero and changes sign at about 1.50 Å. This difference can be easily explained electrostatically. Isolated BF_3 is planar and has a large ^{11}B QCC. The calculated and experimental values are 2.53 (B3LYP/6-311++G**) and 2.64 MHz, respectively.[31] As a B−N bond is formed, the arrangement around the boron

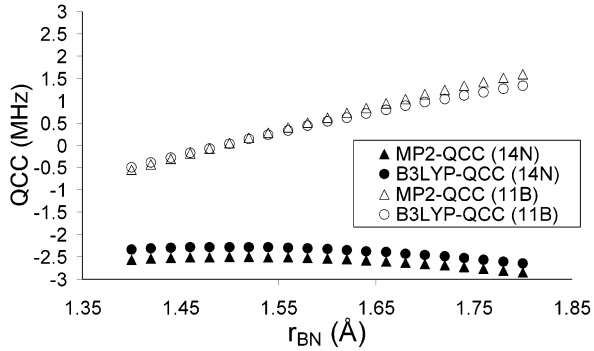

Figure 10. Calculated ^{11}B and ^{14}N nuclear quadrupolar coupling constants for NH_3BF_3 as a function of B−N bond length.

Table 8. Calculated and Experimental Nuclear Quadrupolar Coupling Constants for ND_3BF_3 in the Gas and Solid Phases

	χ (^{11}B)[a]	χ (^{14}N)[a]	χ (^{2}H)[a]
gas-phase microwave[b]	−1.128	−2.324	
calculated using gas-phase structure[c]	−1.132	−2.758	0.252
calculated using solid-state structure[d]	−0.257	−2.27	0.243, 0.272, 0.304
calculated/tetramer A[e]	−0.050		
calculated/tetramer B[f]		−1.63	0.228, 0.260, 0.290
solid-state ^{11}B NMR[g]	±0.080		
solid-state ^{10}B NMR[h]	±0.130		
solid-state ^{2}H NMR[i]			0.184

[a] Quadrupolar coupling constants in MHz. [b] Ref 5. [c] Structure from microwave study. [d] Structure from present neutron diffraction study. [e] See structure in Figure 3A. [f] See structure in Figure 3B. [g] Ref 18. [h] Present work. [i] Present work.

becomes tetrahedral with the fourth atom being the nitrogen. Since fluorine and nitrogen are rather electronegative atoms, there will be some arrangement where the electric field gradients along the three B−F bonds and along the B−N bond will cancel. For B−F bond lengths of about 1.4 Å this occurs when the B−N bond length is about 1.5 Å. In contrast, the geometry of the NH_3 moiety shows relatively little change as the B−N bond is being formed. This together with the lower electron density around the boron results in the ^{14}N QCC being rather insensitive to r_{BN}. Since the electric field gradient at the nucleus, and hence the QCC, is a local molecular electronic property, the presence of the fluorine atoms on the boron has very little effect on the ^{14}N QCC. Now that we have determined the crystal structure of NH_3BF_3, it is possible to calculate the $\chi(^{14}N)$ and $\chi(^{11}B)$ for gas-phase and solid NH_3BF_3. These values are presented in Table 8 together with the previously reported gas-phase microwave and solid-state NMR values. The quality of the spectrum previously presented by Olliges et al. is rather poor.[18] This is primarily due to strong $^{11}B-^{19}F$ and $^{11}B-^{1}H$ dipolar couplings exacerbated by the small ^{11}B QCC (relative to the dipolar couplings). Our attempts to eliminate these dipolar couplings by ^{19}F decoupling and replacement of the protons by deuterons resulted in very modest improvements. An alternative is to examine the ^{10}B spectrum. A ^{10}B spectrum of solid $ND_3{}^{10}BF_3$, with ^{19}F decoupling, is shown in Figure 11. The most prominent feature is the so-called Pake doublet

(31) Casabella, P. A.; Uja, T. *J. Chem. Phys.* **1969**, *50*, 4814.

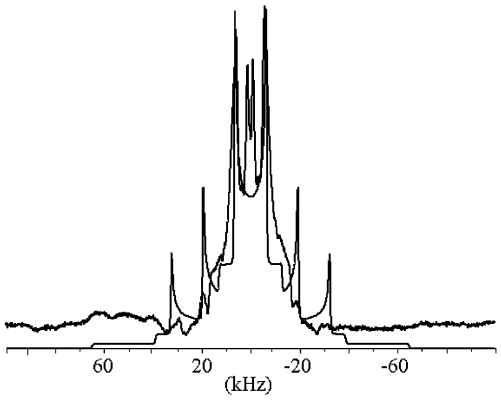

Figure 11. Experimental and simulated ^{10}B NMR line shapes for solid $ND_3{}^{10}BF_3$.

of the central 0↔1 transition. A simulation based on a fit of this feature is also shown. The satellite 1↔2 and 2↔3 transitions do not have the intensity in the experimental spectrum as they do in the simulation. We cannot provide an explanation for this.

As shown in Table 8, our geometry-optimized structure for NH_3BF_3 gave ^{11}B QCC that is in excellent agreement with the observed gas-phase value. Both of these values are about an order of magnitude larger than the two experimental values for the solid state. If a calculation is done on a single molecule with the neutron diffraction structure, the QCC drops to 257 kHz, much closer to the NMR values. If intermolecular N−H···F−B hydrogen-bonding is taken into account by calculating the QCC for the tetramer shown in Figure 3A, the value drops by a further factor of 5−50 kHz, in good agreement with experimental values.

Unfortunately there is no experimental value for the ^{14}N QCC in solid NH_3BF_3. Our calculated single molecule value agrees well with the gas-phase microwave number. Using the solid-state molecular structure reduces the QCC slightly, putting it in better agreement with the microwave value; this is fortuitous. A calculation on the tetramer depicted in Figure 3B causes a significant drop in the ^{14}N QCC. Therefore, one can predict that, because of hydrogen-bonding effects, the solid-state ^{14}N QCC should be at least 1 MHz smaller than the microwave value.

Going from the gas-phase structure to that in the solid and on to tetramer B appears to have very little effect on the deuterium QCC. The result of the last calculation is surprising considering that the deuterons should be directly involved in intermolecular hydrogen-bonding. It has been shown experimentally that hydrogen-bonding reduces the QCC. As pointed out in a previous section of this discussion, the deuterium QCC for ammonia drops from 290.6 kHz in the gas phase to 156 kHz in the solid state.

Chemical Shielding and Chemical Shifts. Calculations (B3LYP/6-311++G(d,p)) of the components of the nuclear magnetic shielding tensor ($\sigma_\perp$ and $\sigma_\parallel$ for boron and nitrogen) as a function of r_{BN} are presented in Figure 12. The variation of shielding with bond length is rather small, being less than 8 ppm in all cases. In addition, the anisotropy in the shielding, $\Delta\sigma = \sigma_\parallel - \sigma_\perp$, is also small. The isotropic shielding is given as $\sigma_{iso} = 1/3(\sigma_\parallel + 2\sigma_\perp)$. The nitrogen shielding values can

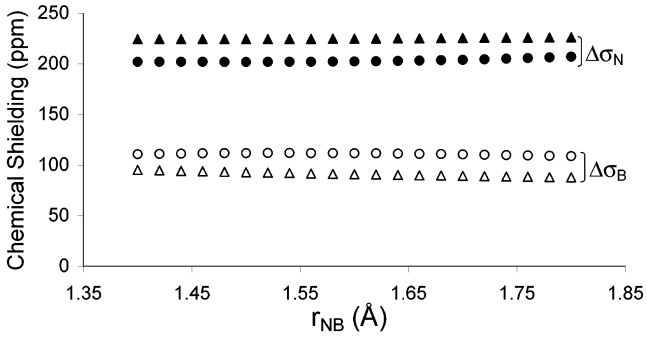

Figure 12. Calculated absolute boron and nitrogen nuclear magnetic shielding values for NH_3BF_3 as a function of B−N bond length.

be converted to the chemical shift scale with respect to liquid CH_3NO_2 according to the equation $\delta = -135.8 - \sigma$.[32] For a single molecule using the solid-state structure a B3LYP/6-311++G(d,p) yields a δ_{iso} of −353.0 ppm. A calculation on the tetramer (Figure 3B), where each NH_3 is surrounded by three hydrogen-bonded NH_3BF_3 molecules, gave a value of −353.6 ppm. As can be seen, the effect of N−H···F−B hydrogen-bonding on the ^{15}N chemical shift is negligible. The components of the chemical shift tensor, $\delta_\parallel$ and $\delta_\perp$, have not been experimentally determined. Unfortunately there is no scale available to convert boron nuclear magnetic shielding to chemical shifts.

Conclusions

Our calculations and measurements, together with earlier measurements, show that the nuclear quadrupolar coupling constant can be a very sensitive probe of electronic, hence molecular, structure. We have successfully solved the neutron diffraction structure for solid NH_3BF_3. The crystal structure shows two important features; a B−N bond length that is much shorter than that in the gas phase and N−H···F−B hydrogen bonds. This structure, together with that from the gas phase, proved very useful for setting up the ab initio calculations. These calculations clearly demonstrated that the changes in the boron and nitrogen quadrupolar coupling constants observed in going from the gas to solid phases is a result of two effects: the large change in the B−N bond length and the N−H···F−B hydrogen-bonding. Calculations employing the gas and solid-state structures also show that the higher barrier to rotation of the NH_3 moiety in the solid is due to these factors. The calculated gas-phase deuterium QCC is much larger than that measured in the solid. Including the abovementioned, effects in the calculations do not bring the two into closer agreement. As yet we have no explanation for this.

Acknowledgment. We thank the Natural Sciences and Engineering Research Council (NSERC) of Canada for financial support. The efforts of Guy Bernard (University of Alberta) and Chris Kirby (University of Western Ontario) toward our attempts to acquire ^{10}B spectra are greatly appreciated.

IC0203771

(32) Ha, T.-K. *Chem. Phys. Lett.* **1986**, *107*, 117.
(33) Spek, A. L. *Acta Crystallogr.* **1990**, *A46*, C34.